Receptor-Regulated Dynamic Interaction between Endothelial Nitric Oxide Synthase and Calmodulin Revealed by Fluorescence Resonance Energy Transfer in Living Cells†

Charles M. Jobin,‡,§ Hongjie Chen,§,|| Alison J. Lin,‡,§ Patrick W. Yacono,‡ Junsuke Igarashi,|| Thomas Michel,*,||,⊥ and David E. Golan*,‡,@

Department of Biological Chemistry and Molecular Pharmacology, Harvard Medical School, Cardiovascular and Hematology Divisions, Brigham and Women's Hospital, and VA Boston Healthcare System, Boston, Massachusetts 02115

Received June 20, 2003; Revised Manuscript Received July 23, 2003

ABSTRACT: The endothelial isoform of nitric oxide synthase (eNOS), a key regulator of vascular tone, is activated in endothelial cells by diverse Ca^{2+}-mobilizing agonists, including vascular endothelial growth factor (VEGF). Although the activation state of eNOS and the subcellular localization of the enzyme are both highly regulated, the relationship between enzyme activity and subcellular targeting remains obscure. We aim here to elucidate this relationship by direct dynamic imaging analysis of Ca^{2+}/CaM-dependent eNOS activation in living endothelial cells, using high-resolution confocal microscopy and donor dequenching fluorescence resonance energy transfer (FRET) techniques. Confocal images show a complex pattern of eNOS subcellular distribution; the enzyme is concentrated in both the plasma membrane and internal membranes, with robust expression in the perinuclear region. We construct a fusion protein between eNOS and the FRET-based calcium sensor cameleon, and analyze the temporal and spatial pattern of VEGF-mediated calcium mobilization using donor dequenching FRET methods. We find that VEGF promotes rapid mobilization of intracellular calcium throughout the regions of the cell in which eNOS is distributed. We further create a series of fusion proteins and use FRET imaging methods to study the interactions between eNOS and its obligate allosteric activator protein calmodulin. We clone the FRET acceptor EYFP (enhanced yellow fluorescent protein) at the C-terminus of calmodulin, and the FRET donor ECFP (enhanced cyan fluorescent protein) into eNOS at a site adjacent to its calmodulin-binding domain. FRET imaging analysis of individual endothelial cells cotransfected with eNOS−ECFP and calmodulin−EYFP shows that VEGF induces interactions between eNOS and calmodulin wherever both are present in the cell. Our studies provide evidence that the pool of rapidly responsive receptor-activated eNOS is distributed throughout endothelial cells in both plasma membrane and internal membrane structures, and that this distribution parallels the localization of agonist-induced intracellular Ca^{2+} changes in the vicinity of eNOS.

The endothelial isoform of NO synthase (eNOS)[1] is a critical signaling molecule in vascular endothelial cells. eNOS-mediated NO production is highly regulated by a series of transcriptional, posttranscriptional, and posttranslational events, including acylation, phosphorylation, protein−protein interactions, and others (*1*−*3*). The subcellular distribution of eNOS is also complex in native endothelial cells, where the enzyme is localized in both plasma membrane and internal membrane structures. It has recently become apparent that the subcellular compartmentalization of eNOS has a significant impact on enzyme function (*4*−*7*). Establishing the nature of the relationships among eNOS localization, activation, and protein−protein interactions has therefore become an important challenge (*8*−*10*).

In vascular endothelial cells, eNOS is activated by diverse Ca^{2+}-mobilizing cell surface receptors and by hemodynamic shear stress. The synthesis of NO by eNOS depends on the binding of the enzyme to calmodulin, a calcium regulatory protein that serves ubiquitously as a cellular calcium sensor to regulate a variety of metabolic and signaling pathways (*11*). Ca^{2+} binding to calmodulin stimulates conformational changes in the protein, leading to the exposure of hydro-

† This work was supported by NSF Grant EEC-9986821 and NIH Grants HL32854 and HL15157 to D.E.G., NIH Grants GM36259 and HL46457 to T.M., and a Burroughs Wellcome Fund Scholar Award to T.M. A.J.L. was supported by NIH Training Grant T32ES07155.

* To whom correspondence should be addressed. T.M.: Cardiovascular Division, Brigham and Women's Hospital, 75 Francis St., Boston, MA 02115. Phone: (617) 732-7376. Fax: (617) 732-5132. E-mail: michel@calvin.bwh.harvard.edu. D.E.G.: Department of Biological Chemistry and Molecular Pharmacology, Harvard Medical School, 250 Longwood Ave., Boston, MA 02115. Phone: (617) 432-2256. Fax: (617) 432-3833. E-mail: dgolan@hms.harvard.edu.

‡ Harvard Medical School.

§ These authors contributed equally to this work.

|| Cardiovascular Division, Brigham and Women's Hospital.

⊥ VA Boston Healthcare System.

@ Hematology Division, Brigham and Women's Hospital.

[1] Abbreviations: BAEC, bovine aortic endothelial cells; CaM, calmodulin; ECFP, enhanced cyan fluorescent protein; eNOS, endothelial nitric oxide synthase; EYFP, enhanced yellow fluorescent protein; FRET, fluorescence resonance energy transfer; NO, nitric oxide; ΔeNOS, deletion mutant of eNOS with the calmodulin binding site removed.

10.1021/bi035066w CCC: $25.00
Published on Web 09/13/2003

phobic surfaces that bind to specific amphipathic helical domains in target proteins. Although the biochemistry of eNOS activation by Ca^{2+}/calmodulin has been extensively characterized, the cell biology of this regulation is less well understood. One important unresolved question concerns the ability of eNOS molecules throughout the cell to interact with Ca^{2+} and calmodulin. It is possible, for example, that only eNOS molecules localized to the plasma membrane are capable of binding calmodulin, or that only eNOS molecules in internal structures are accessible to cytoplasmic Ca^{2+}/calmodulin. To answer these questions, we use fluorescence resonance energy transfer (FRET) techniques to explore, in real time, the receptor-mediated activation of eNOS by calcium and calmodulin in cultured live endothelial cells.

FRET refers to the nonradiative transfer of energy between two fluorophores, where the emission spectrum of one, the donor, overlaps significantly with the excitation spectrum of the other, the acceptor (*12*−*16*). The occurrence of FRET is highly dependent on the dipole orientations of the fluorophores and on the distance between the fluorophores. The efficiency of FRET is inversely proportional to the sixth power of the fluorophore−fluorophore separation distance, allowing the detection and analysis of protein−protein interactions on the scale of 10−100 Å. FRET-based analysis can therefore provide greater specificity and higher spatial resolution than conventional light microscopy in studying the physical interactions between fluorescently labeled cellular components. Tsien and colleagues have developed and characterized spectral variants of the enhanced green fluorescent protein (EGFP) that are especially useful for FRET applications, and have used digital imaging methods to detect FRET in cells transfected with cDNAs that encode chimeric proteins in which the protein(s) of interest is fused to specific EGFP variants (*15*, *16*). A particularly robust FRET pair consists of enhanced cyan fluorescent protein (ECFP) as the donor and enhanced yellow fluorescent protein (EYFP) as the acceptor. These important advances, along with recent developments in optics and image processing, have facilitated studies of protein−protein interactions in living cells.

Here, we use GFP fusion proteins, confocal microscopy, and sensitive FRET imaging methods to study the receptor-mediated, calcium-dependent interaction between eNOS and calmodulin in living native endothelial cells. We use FRET imaging analysis to assess not only the occurrence but also the subcellular location of this protein−protein interaction. We find that receptor-mediated eNOS activation takes place at all locations within the cell, and that enzyme activation correlates spatially and temporally with changes in calcium levels in the vicinity of the eNOS molecules.

MATERIALS AND METHODS

Materials. DNA restriction enzymes were purchased from New England Biolabs, Inc. (Beverly, MA). *Pfu* DNA polymerase was from Stratagene (La Jolla, CA). eNOS monoclonal antibody was from Transduction Laboratories (Lexington, KY); enhanced green fluorescent protein (EGFP) antibody was from Clontech Laboratories, Inc. (Palo Alto, CA). Fetal bovine serum was from Hyclone (Logan, UT). Other cell culture reagents and media were from Invitrogen (Carlsbad, CA). Fugene6 transfection reagent was from Roche Molecular Biochemicals (Indianapolis, IN). Fluo3/AM was from Molecular Probes, Inc. (Eugene, OR). All other reagents were from Sigma-Aldrich, Inc. (St. Louis, MO).

Plasmid Construction. Fluorescent protein plasmids pECFP-C1 and pEYFP-N1 were purchased from Clontech Laboratories, Inc. The eukaryotic expression plasmid encoding bovine wild-type eNOS cDNA has been described previously (*17*). YC2.1, the cDNA plasmid that encodes cameleon and contains the sequence for calmodulin (*15*), was a kind gift of R. Y. Tsien (Howard Hughes Medical Institute, University of California, San Diego, CA). Polymerase chain reaction-based approaches were used to create compatible restriction enzyme sites that would permit construction of chimeric cDNAs for FRET. The DNA sequences of all constructs generated or modified by PCR were verified by nucleotide sequence analysis. In addition, the expression levels of these fusion constructs were validated in transient transfection experiments in COS-7 cells followed by immunoblot analyses, and eNOS activity of the constructs was determined using the [^{3}H]arginine−[^{3}H]citrulline assay, as previously described (*18*).

The eNOS−EGFP construct (eNOS−EGFP) was constructed as previously reported (*6*). To create the fusion construct encoding the eNOS−ECFP construct (eNOS−ECFP), the pECFP-C1 cDNA was amplified by PCR using the plasmid pECFP-C1 as a template, with the forward primer 5′-CATAGGAAGATCTCTGGGGGGATGGTGAG-CAAGGGC-3′ and the reverse primer 5′-GTTACCTA-GATCTTGCCGCCCTTGTACAGCTCGTC-3′. These amplimers added *Bgl*II restriction enzyme sites onto either end of the ECFP sequence, as well as a short linker region comprising two glycine residues. The resulting PCR products were digested with *Bgl*II and inserted into the *Bgl*II site within the eNOS cDNA, which is located immediately 3′ to the calmodulin binding site of eNOS (*19*). The eNOS−ECFP chimeric construct was predicted to encode a protein with a molecular mass of 163 kDa (Figure 1).

Construction of the CaM−EYFP chimera involved ligating the EYFP cDNA to the 3′-terminus of calmodulin. To generate *Eco*RI and *Age*I restriction enzyme sites at the 5′- and 3′-termini, respectively, of the calmodulin sequence, we performed PCR (using the calmodulin-containing YC2.1 plasmid as a template) with the forward primer 5′-CGGAATTCGCCACCATGGGCCATGACCAACTGAC-AGAAG-3′ and the reverse primer 5′-CGAACACCGGTC-CCTTTGCTGTCATCATTTG-3′. The amplified product was digested with *Eco*RI and *Age*I, and then cloned into the pEYFP-N1 plasmid to generate the CaM−EYFP chimeric construct with a predicted molecular mass of 42 kDa (Figure 1).

The deletion mutant encoding ΔeNOS−ECFP was made by replacing the fragment between the *Sca*I and *Bgl*II restriction enzyme sites within eNOS cDNA with the ECFP cDNA amplified by PCR from pECFP-C1. The upstream *Sca*I site and the sequences encoding two glycine residues were included in the forward primer 5′-GTCAAAAGTAC-TACGGTGGAATGGTGAGCAAGGGCGAG-3′. The reverse primer was the same as that used in making eNOS−ECFP (Figure 1). ΔeNOS−ECFP (121 kDa) lacks amino acid residues 136−506 of eNOS, thereby removing the putative calmodulin binding site (*19*) while retaining se-

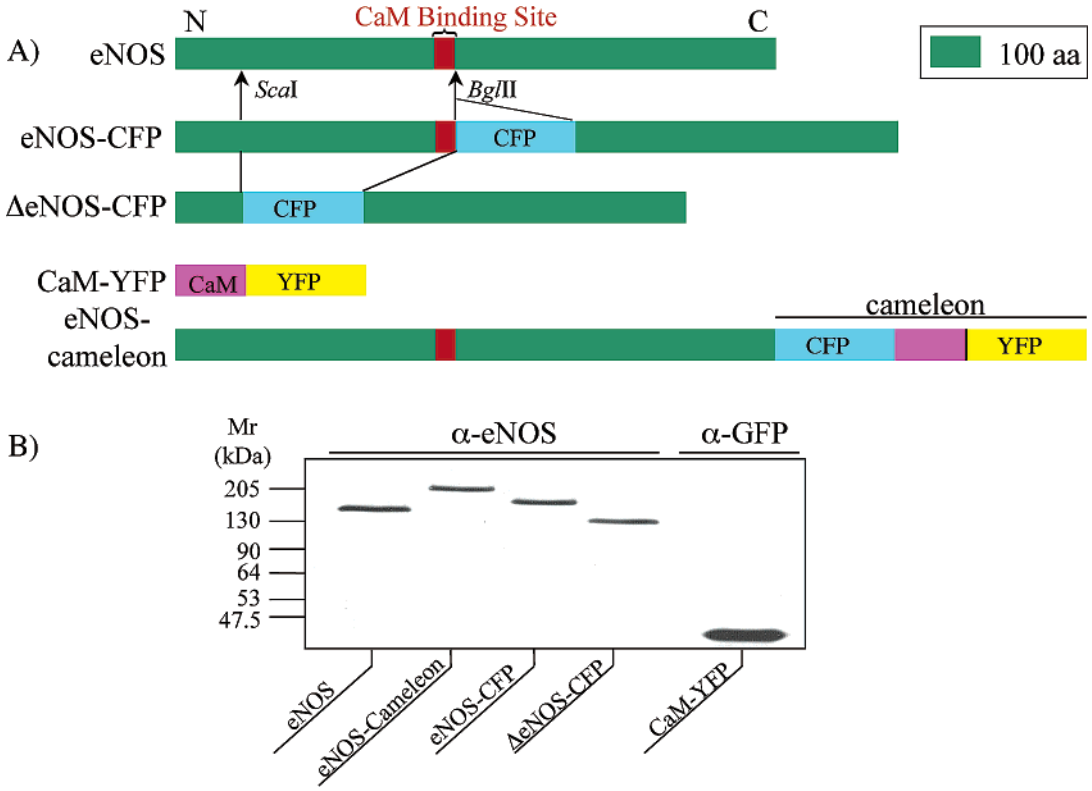

FIGURE 1: eNOS and calmodulin fusion constructs for analysis of FRET. (A) Schematic of wild-type eNOS protein and its fusion proteins with the fluorophores ECFP and EYFP. The CaM-binding site of eNOS is located N-terminal to a *Bgl*II restriction site in the eNOS cDNA. We created *Bgl*II restriction sites at the termini of the ECFP cDNA using PCR, and inserted the ECFP cDNA into the *Bgl*II site of eNOS to yield the eNOS−ECFP fusion protein. CaM−EYFP was made by ligating EYFP cDNA to the 3′ end of calmodulin cDNA after compatible restriction enzyme sites had been added to the termini of calmodulin cDNA, as described in Materials and Methods. As a negative control, we used an eNOS deletion mutant (ΔeNOS) that lacked the calmodulin binding site; ECFP was cloned into the same restriction site as that used for wild-type eNOS. The cameleon construct was a calcium-sensing FRET construct (*15*) that we ligated at the 3′-terminus of eNOS to make an eNOS−cameleon chimera. (B) Immunoblots of COS-7 cells transfected with cDNAs encoding wild-type eNOS, eNOS−ECFP, ΔeNOS−ECFP, cameleon−eNOS, and CaM−EYFP. Lysates of transfected cells were analyzed in immunoblots probed with anti-eNOS antibody (for eNOS-containing constructs) or with anti-EGFP antibody (for CaM−EYFP).

quences essential for proper subcellular targeting of eNOS (*20*).

The eNOS−cameleon construct (207 kDa) was generated by using PCR to produce *Bam*HI and *Not*I restriction sites flanking the cameleon sequence within the plasmid YC2.1. The upstream primer had the sequence 5′-GCAAGGATC-CAGGAGGTATGGTGAGCAAGGGCGAGG-3′, and the downstream primer was 5′-AAGGAAAAAAGCGGCCGCTT-TACTTGTACAGCTCGTCCA-3′. The amplified product was digested with *Bam*HI and *Not*I, and ligated to the 3′-carboxyl terminus of eNOS (Figure 1).

Cell Culture and Transfection. Bovine aortic endothelial cells (BAEC), from Cell Systems (Kirkland, WA), were maintained in culture in Dulbecco's modified Eagle's medium (DMEM) containing 10% FBS (complete medium), as described previously (*19*). BAEC were studied between passages 6 and 9. The day before transfection, cells were split at a ratio of 1:8 and plated onto gelatin-coated chambers in two-well coverslips (Nunc-LabTek, Rochester, NY). Transient transfection of BAEC with plasmid DNA was performed using Fugene6, according to the manufacturer's protocol. Cells were transfected with both CaM−EYFP (0.2 μg per two wells) and eNOS−ECFP (0.8 μg) or ΔeNOS−ECFP (0.8 μg), or with eNOS−ECFP (1 μg), CaM−EYFP (0.2 μg), or eNOS−cameleon (1 μg) alone. Transfection conditions were optimized in preliminary experiments; the transfection efficiency in experiments reported here was 30−50%. Approximately 8 h after transfection, the culture medium was replaced with complete medium without phenol red; the cells were studied 24−36 h after transfection.

Measurement of the Level of Intracellular Calcium Using Fluo-3. Intracellular calcium concentrations were determined using the indicator dye Fluo-3 and our previously described methods (*5*) employing a stage scanning laser fluorescence microscope (Meridian Instruments Ultima, Okemos, MI). A 180 μm × 180 μm field was scanned with a step size of 2 μm; the complete field was scanned every 30 s for 10−25 min after addition of agonist. Each field contained 10−15 cells, and the fluorescence signal was quantified using MetaMorph software (Universal Imaging Corp., West Chester, PA).

High-Resolution Fluorescence Microscopy. High-resolution imaging was performed in the Nikon Imaging Center at Harvard Medical School using both epifluorescence and confocal techniques. A Nikon TE2000U inverted microscope stand was used in combination with the PerkinElmer Ultraview spinning disk confocal attachment, Hamamatsu Orca ER-cooled CCD camera, and Prior Scientific OptiScan motorized stage (all from Micro Video Instruments, Inc., Avon, MA). Data were acquired using MetaMorph image acquisition software in stacks of optical slices, each of which represented the $x-y$ image at a particular z. These stacks were then processed using Autoquant deconvolution software (Meyer Instruments, Inc., Houston, TX) and reconstructed

to form a three-dimensional representation of the cells of interest.

FRET Microscopy. Cells were observed using an epifluorescence inverted microscope (Nikon Diaphot-300) equipped with a 100 W mercury lamp, a 60x/1.4NA plan-APO objective, differential interference contrast optics, and donor (CFP) and acceptor (YFP) filter sets (Omega Optical, Brattleboro, VT). The CFP set included a 440/20 nm excitation filter, a 455 nm long-pass (LP) dichroic mirror, and a 480/30 nm emission filter; the YFP set included a 500/25 nm excitation filter, a 525 nm LP dichroic mirror, and a 545/35 nm emission filter. Images were captured using a liquid-cooled CCD camera equipped with a KAF-1400 chip (model CH250, Photometrics, Tucson, AZ) and operated by the MetaMorph imaging system and a shutter driver (model D122, UniBlitz, Rochester, NY), as described previously (*21*).

To detect FRET between cotransfected intracellular proteins conjugated to EGFP variants, the donor and acceptor signal intensity and spectral overlap must be sufficient. Typically, FRET microscopy has involved illuminating the specimen at a wavelength that excites the donor fluorophore, and then assembling a digital cellular image by quantifying, pixel by pixel, the FRET signal intensity at the emission wavelength of the acceptor fluorophore. At the low signal intensities characteristic of transfected native endothelial cells, the detection of FRET is particularly hampered by the presence of overlap between donor and acceptor emission spectra. In preliminary experiments using a conventional FRET filter set (440/20 nm excitation filter, 525 nm LP dichroic mirror, and 545/35 nm emission filter), we found that both ECFP and EYFP independently contributed to the signal in the FRET channel from endothelial cells cotransfected with eNOS−ECFP and CaM−EYFP. This result made it difficult to quantify FRET by measuring the sensitized emission of the EYFP acceptor fluorophore. Therefore, instead of measuring FRET efficiency as the increase in sensitized *acceptor* fluorescence emission, we adapted methods for monitoring FRET by quantifying the emission from the *donor* fluorophore before and after photobleaching of the acceptor fluorophore (*22*). In this "donor dequenching after acceptor photobleaching" method, when FRET is present, the intensity of donor emission (in this case, ECFP) increases after a nearby acceptor fluorophore (EYFP) is inactivated by irreversible photobleaching. Thus, a combination of filter sets and exposure times was chosen to minimize EYFP excitation and emission in the CFP channel, allowing for reliable quantification of ECFP emission. Using the CFP filter set, there was no observable emission above background levels in cells transfected with CaM−EYFP alone; conversely, there was no signal obtained using the YFP filter set from cells transfected with eNOS−ECFP alone. These methods allowed accurate quantification of ECFP dequenching in live BAEC.

Calculation of FRET Efficiency. The simplest calculation of FRET efficiency by the donor dequenching method assumes that all of the acceptor fluorophores are photobleached. In this case, the FRET efficiency (*E%*) is given by

$$E\%\ (\text{total photobleaching}) = \frac{\Delta C}{C_f} \times 100 = \left(\frac{C_f - C_i}{C_f}\right) \times 100 \quad (1)$$

where C_i and C_f are the fluorescence intensities of ECFP before (initial) and after (final) photobleaching of EYFP, respectively. When only a fraction of the EYFP molecules are photobleached, the subsequent increase in ECFP fluorescence is only a fraction of ΔC. We define a parameter β as being equal to Y_f/Y_i, where Y_i and Y_f are the fluorescence intensities of EYFP before and after photobleaching, respectively, such that $\alpha = 1 - \beta$ is the fraction by which the acceptor intensity is decreased due to photobleaching. C_f can then be expressed in terms of C^*_f, the ECFP intensity after partial photobleaching of EYFP

$$C_f = \frac{C^*_f - \beta C_i}{\alpha} \quad (2)$$

Combining eqs 1 and 2, we obtain

$$E\%\ (\text{partial photobleaching}) = \left(1 - \frac{\alpha C_i}{C^*_f - \beta C_i}\right) \times 100 \quad (3)$$

Quantification of FRET by Assessment of Donor Dequenching after Acceptor Photobleaching. For each sample, representative cells were chosen at random. Experiments were repeated at least three times on different days. MetaMorph software was used to collect 400 pixel × 400 pixel digital images of cellular ECFP and EYFP fluorescence at 12 bit resolution; images were recorded both before and after photobleaching of EYFP. A 32× neutral density filter was used in the excitation light path; exposure times were 1.2 s for ECFP images and 0.8 s for EYFP images. These conditions were found to cause negligible photobleaching of either ECFP or EYFP during image acquisition.

Selective and irreversible acceptor photobleaching was achieved by exposing cells for 10 s to excitation light through the YFP filter set without a neutral density filter. The extent of EYFP photobleaching was measured to be approximately 80% of the cellular EYFP in each experiment, with each cell serving as its own reference. Under these conditions, there was no measurable photodamage to the cells and no measurable photobleaching of the ECFP.

MetaMorph software was used to analyze the ECFP and EYFP images before and after partial photobleaching of EYFP. For each image, the integrated fluorescence intensity was recorded in arbitrary units that were comparable within a given experiment. The background signal was removed using a median filter; application of the MetaMorph shading correction further eliminated image artifacts caused by camera noise. Masks made from the postbleach ECFP image and the prebleach EYFP image were then applied to the prebleach ECFP image and the postbleach EYFP image, respectively. In this manner, Y_i, Y_f, C_i, and C^*_f were obtained, and the FRET efficiency *E%* was calculated using eq 3. Mean values of *E%* for individual experiments were plotted, with error bars denoting the respective standard errors of the mean. Differences between experimental results were analyzed using the unpaired *t* test assuming unequal vari-

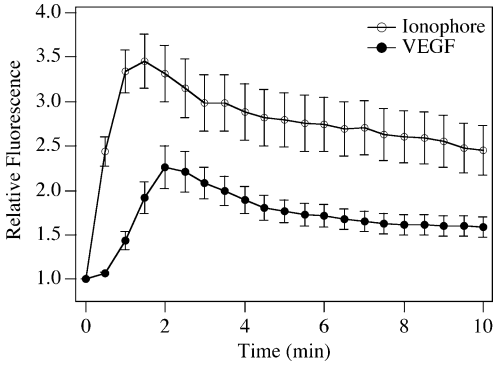

FIGURE 2: Time course of intracellular calcium response to stimulation with the calcium ionophore or VEGF. BAEC on coverslips were incubated with the Ca^{2+}-sensitive dye Fluo-3 and then analyzed by digital imaging fluorescence microscopy in real time following the addition of VEGF (20 ng/mL) or the calcium ionophore A23187 (10 μM). Data points represent the mean ± standard error of the mean for 13−24 individual cells analyzed in three independent experiments. Data are shown as the integrated intensity of Fluo-3 fluorescence for each cell, expressed relative to a fluorescence intensity of 1 at time zero for that cell.

ances. A two-tailed *p* value of less than 0.02 was considered to be statistically significant.

MetaMorph software was also used to measure the fluorescence intensities of individual pixels within the pre- and post-photobleach ECFP and EYFP images. Equation 3 was used to calculate the FRET efficiency *E%* for each pixel; *E%* was set to zero for all pixels in which the post-photobleach change in ECFP or EYFP fluorescence was less than or equal to that determined in cell-free regions. An appropriate scaling factor was applied to stretch the range of *E%* values onto a 16 bit pseudocolor scale (0−65535), to achieve the best contrast in a two-dimensional image. In this manner, a pixel-by-pixel representation of FRET efficiencies (called a "FRET image") was constructed, aiding the visualization of *E%* at all locations in the cell. Because cell movement between pre- and post-photobleach images could confound the construction of the FRET image, we analyzed only FRET images in which there was no apparent cell movement during the experiment.

RESULTS

We performed a series of interrelated experiments to explore the temporal and spatial pattern of calcium mobilization and eNOS activation in bovine aortic endothelial cells (BAEC). The eNOS agonist vascular endothelial growth factor (VEGF) and the calcium ionophore A23187 each promote the rapid and robust activation of eNOS in these cells (*3*). We first used the cell-permeable calcium-sensitive dye Fluo-3 to characterize intracellular calcium responses (*5*), and monitored Ca^{2+} transients in real time following the addition of VEGF or the calcium ionophore. As shown in Figure 2, both VEGF and the calcium ionophore induced a rapid increase in intracellular calcium levels; the calcium response to VEGF was slightly delayed and smaller in magnitude than that elicited by the calcium ionophore. The time course of the agonist-activated calcium response was consistent with the kinetics of NO production in BAEC stimulated with VEGF (*23*).

We next analyzed eNOS localization and activation in individual endothelial cells, using high-resolution imaging

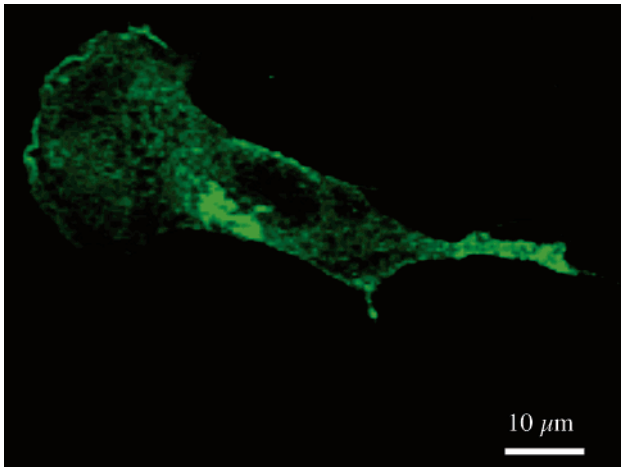

FIGURE 3: Confocal image of BAEC transfected with eNOS−EGFP. Shown as the maximum projection representation of a deconvolved confocal *z*-stack image is an endothelial cell transfected with cDNA encoding the eNOS−EGFP fusion protein, and analyzed using a fluorescence spinning disk confocal microscope. The image is representative of results obtained in three independent experiments.

techniques to study eNOS tagged with the fluorescent marker protein EGFP. Because many signaling proteins are targeted aberrantly when introduced into heterologous cell systems, we chose to analyze the distribution of eNOS−EGFP by performing transient transfection experiments in native BAEC. This cell type represents the archetypal cultured endothelial cell, in which transient expression of exogenous plasmid cDNA constructs can be achieved using liposome-based transfection reagents. We started by constructing the fusion protein eNOS−EGFP for localization studies (*6*). As shown in Figure 3, confocal microscopy images of BAEC transfected with eNOS−EGFP revealed a complex subcellular eNOS distribution pattern. eNOS−EGFP was distributed along the plasma membrane as well as internal membranes, particularly in the perinuclear region. This complex subcellular localization of eNOS−EGFP reproduced the localization of native eNOS analyzed using immunofluorescence techniques (*5*), thus establishing the validity of using the transfected fusion protein as a surrogate for the native protein.

Although the subcellular distribution of eNOS significantly affects many characteristics of eNOS signaling (*6*, *24*), the relationships among eNOS targeting, enzyme activity, and local calcium concentration are less well understood. We therefore explored whether calcium concentrations in the vicinity of eNOS molecules in the various subcellular locations were uniformly responsive to agonist activation. For this purpose, we created a fusion protein (Figure 1A) with the C-terminus of eNOS and the FRET-based calcium reporter protein cameleon (gift of R. Tsien; *15*). The cameleon molecule contains a central domain comprising calmodulin and the calmodulin-binding peptide M13, flanked on one side by the FRET donor ECFP and on the other side by the FRET acceptor EYFP. In the presence of Ca^{2+}, alterations in the conformation of cameleon permit the calmodulin and the calmodulin-binding domains to interact, leading to sufficiently close apposition of ECFP and EYFP such that FRET occurs between these two fluorophores (*15*). The enzyme activity of the eNOS−cameleon construct was identical to that of native eNOS, as assessed in transient

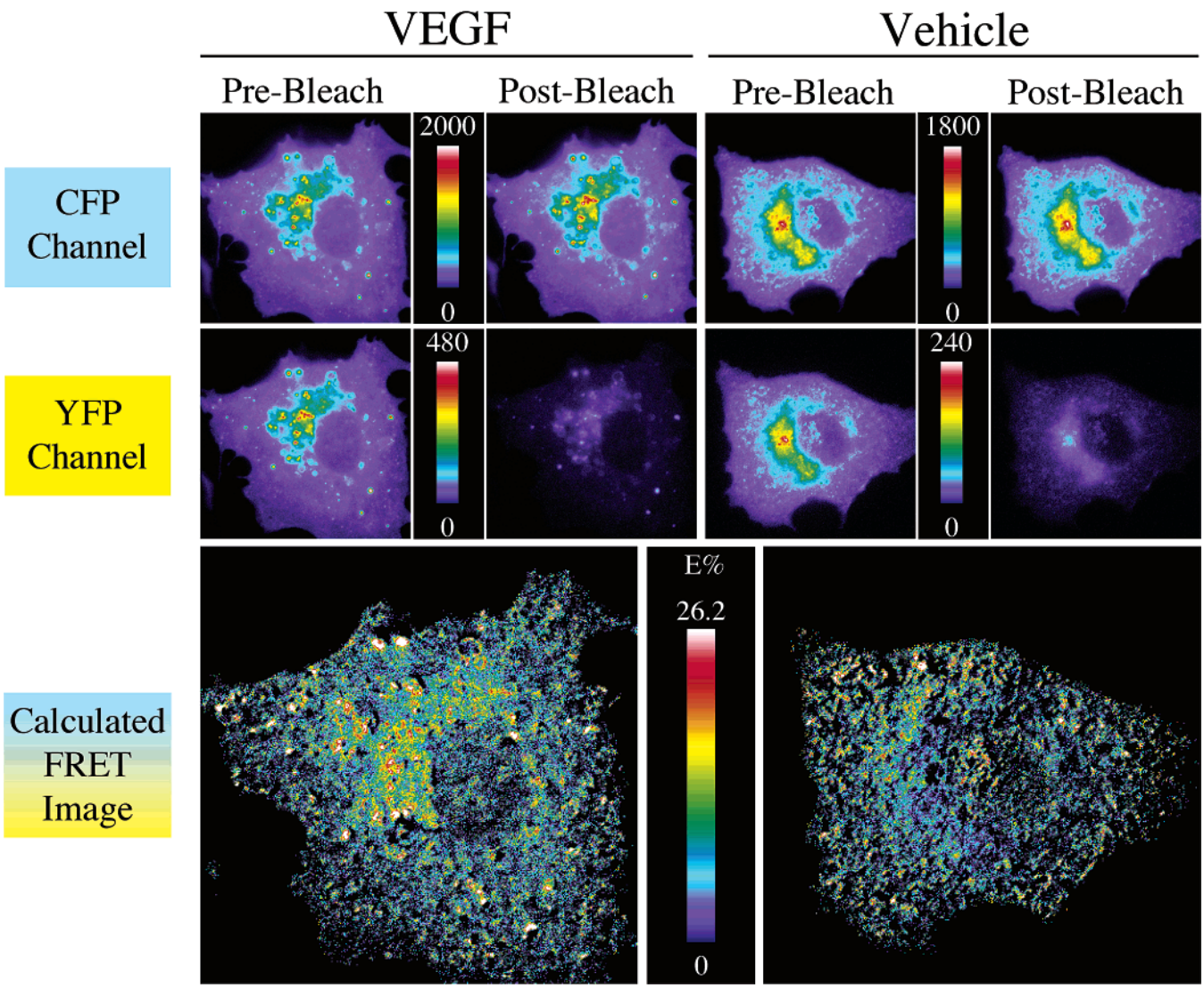

FIGURE 4: FRET imaging of the accessibility of eNOS to intracellular calcium using the eNOS−cameleon fusion protein. BAEC were transfected with eNOS fused to the calcium-sensitive FRET detector cameleon, and FRET images were obtained using donor dequenching approaches in live cells. Transfected BAEC were analyzed for FRET following the addition of VEGF (20 ng/mL, left panels) or vehicle (right panels). Cells were imaged using an epifluorescence microscope with CFP and YFP filter sets as described in the text, and images were captured using a CCD camera. To quantify FRET by donor dequenching, separate prebleach digital images were acquired from the CFP and YFP channels. The EYFP fluorophore was then selectively photobleached, and a pair of postbleach digital images were captured. Quantitative comparison of the prebleach and postbleach EYFP fluorescence images reflected the photobleaching efficiency, and quantitative comparison of the prebleach and postbleach ECFP images yielded the extent of donor dequenching. In this approach, each cell served as its own reference. Data were processed using the FRET equation, as described in detail in the text, to calculate the FRET efficiency (*E*%) for each cell, and analyzed pixel by pixel to generate the calculated FRET image shown at the bottom of each panel. The top panels show images captured using the ECFP filter set before and after photobleaching of EYFP; the middle panels show the corresponding images captured using the YFP filter set before and after photobleaching. Note the increase in ECFP channel fluorescence throughout the cell after photobleaching of EYFP in cells treated with VEGF (20 ng/mL) for 5 min. The lower panels display the calculated FRET image for the same cell.

transfection experiments in COS-7 cells (data not shown). The eNOS−cameleon fusion protein was used to probe the regulation of intracellular calcium concentrations in the vicinity of eNOS molecules throughout the cell.

FRET imaging of intracellular Ca^{2+} was performed using the donor dequenching after acceptor photobleaching method, as described in detail in Materials and Methods. We measured the extent of intramolecular FRET for eNOS−cameleon in transfected live BAEC by quantifying the amount of donor (ECFP) dequenching after selective acceptor (EYFP) photobleaching. Using the CFP and YFP filter sets, a series of digital images were obtained before and after photobleaching of the acceptor fluorophore. The extent of EYFP (acceptor) photobleaching was obtained by comparing the prebleach and postbleach EYFP fluorescence intensities in the same cell. The extent of donor (ECFP) dequenching was measured by comparing the ECFP fluorescence intensities before and after EYFP photobleaching in the same cell. The prebleach and postbleach EYFP and ECFP fluorescence intensities were used in eq 3 to calculate the FRET efficiency for each pixel, and thereby to generate a FRET image of the cell (Figure 4).

We used VEGF to activate eNOS, as we had found previously (*25*) that VEGF stimulates the most robust receptor-mediated activation of eNOS in these cells. Treatment with either VEGF (Figure 4) or the calcium ionophore

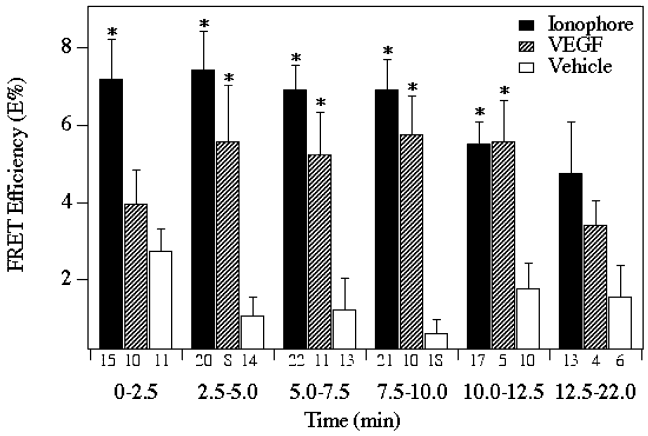

FIGURE 5: Time course of eNOS−calmodulin FRET after stimulation with the calcium ionophore or VEGF. Shown are the FRET efficiencies determined in BAEC cotransfected with eNOS−ECFP and CaM−EYFP and then stimulated with VEGF (20 ng/mL) or the calcium ionophore A23187 (10 μM) for the indicated periods of time. The experiment was repeated three times with equivalent results; in each experiment, 10−15 cells were analyzed. The total number of cells analyzed for each condition is shown under each bar. Error bars represent the standard error of the mean. Asterisks reflect values significantly different from the time zero control at the $p < 0.02$ level.

A23187 (not shown) induced marked increases in FRET signals in BAEC that had been transfected with eNOS−cameleon. The pattern of eNOS-associated Ca^{2+} transients monitored using FRET methods (data not shown) had a time course similar to that of the increases in the levels of intracellular Ca^{2+} monitored using the Ca^{2+}-sensitive dye Fluo-3 (Figure 2). As shown in Figure 4, there was a robust FRET response to VEGF throughout all regions of the cell, indicating that eNOS populations throughout the cell were uniformly accessible to Ca^{2+}. A similar pattern was seen in response to treatment with the calcium ionophore (data not shown). Thus, VEGF promotes increases in the level of intracellular calcium throughout all endothelial cell compartments in which eNOS is localized.

We next sought to determine whether increases in the level of intracellular calcium in the vicinity of eNOS were associated with functional activation of the protein. We used a FRET-based experimental approach, in which the donor was a chimeric eNOS−ECFP fusion protein and the acceptor was a calmodulin−EYFP fusion protein (Figure 1A). The calmodulin binding site of eNOS is located near the middle of the protein, immediately adjacent to a propitious restriction enzyme site. PCR was used to modify the termini of cDNA encoding ECFP to permit its insertion into the eNOS cDNA at this site. All constructs generated by PCR-based approaches were validated by nucleotide sequence analysis, and expression of fusion proteins of the correct molecular size in transfected cells was confirmed by immunoblot analysis (Figure 1B). The chimeric eNOS−ECFP retained enzymatic activity that was approximately 10% of that of the wild-type enzyme, as determined in transient transfection experiments in COS-7 cells (data not shown). Like eNOS−EGFP (Figure 3), eNOS−ECFP manifested a subcellular pattern of localization in transfected BAEC similar to that of wild-type eNOS (Figure 7; see also hydrodynamic analyses in ref *18*).

The FRET acceptor molecule EYFP was cloned as a fusion protein with calmodulin (CaM) to generate the CaM−EYFP fusion construct (Figure 1A). In this construct, EYFP was fused at the 3′-terminus (carboxyl) of calmodulin, again using PCR to generate propitious restriction sites at the termini of the fluorophore cDNA.

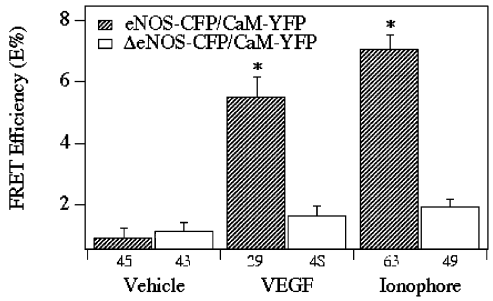

FIGURE 6: Induction of FRET between eNOS−ECFP and CaM−EYFP by stimulation with the calcium ionophore or VEGF. Shown are the FRET efficiencies between cotransfected CaM−EYFP and either eNOS−ECFP (cross-hatched bars) or the deletion mutant ΔeNOS−ECFP (white bars). Cotransfected BAEC were treated for 2 min with the calcium ionophore A23187 (10 μM) or for 5 min with VEGF (20 ng/mL). The experiment was repeated three times with equivalent results; in each experiment, 10−15 cells were analyzed. The total number of cells analyzed for each condition is shown under each bar. Error bars represent the standard error of the mean. Asterisks reflect values significantly different from the vehicle control at the $p < 0.02$ level.

Having constructed and validated these fusion proteins, we measured the extent of intermolecular FRET between eNOS−ECFP and CaM−EYFP in transfected live BAEC by quantifying the amount of donor (ECFP) dequenching after selective acceptor (EYFP) photobleaching, as described above. We found that, when two plasmids that separately encoded ECFP and EYFP fusion proteins were cotransfected, more than 95% of the successfully transfected cells expressed both plasmids. We first analyzed the time course of the eNOS−calmodulin interaction in live BAEC that had been cotransfected with the eNOS−ECFP and calmodulin−EYFP constructs. As shown in Figure 5, the FRET response to VEGF was observed after a short delay (~2.5 min), while the response to the calcium ionophore was both more rapid and more robust. For both VEGF and calcium ionophore stimulation of live BAEC, the time course of the eNOS−calmodulin interaction paralleled the agonist-induced increase in the level of intracellular Ca^{2+} (Figure 2).

A series of control experiments was performed to establish the specificity of the eNOS−calmodulin interaction FRET signal. No FRET signal was observed when the eNOS−ECFP construct was transfected without the CaM−EYFP construct; this control showed that the FRET signal was not derived from self-dequenching of the donor fluorophore after photobleaching through the YFP filter set, but rather depended on the presence of the CaM−EYFP FRET acceptor. Further, there was no FRET response in the absence of added VEGF or calcium ionophore (Figure 6). The most compelling control experiment used, in place of eNOS−ECFP, a fusion protein in which ECFP was cloned into an eNOS deletion mutant that lacked the calmodulin binding site (Figure 1). This ΔeNOS−ECFP construct exhibited no eNOS enzymatic activity in transient transfection experiments in COS-7 cells, although its subcellular localization in transfected BAEC was similar to that of wild-type eNOS (data not shown). As shown in Figure 6, there was no FRET signal between ΔeNOS−ECFP and CaM−EYFP in cotrans-

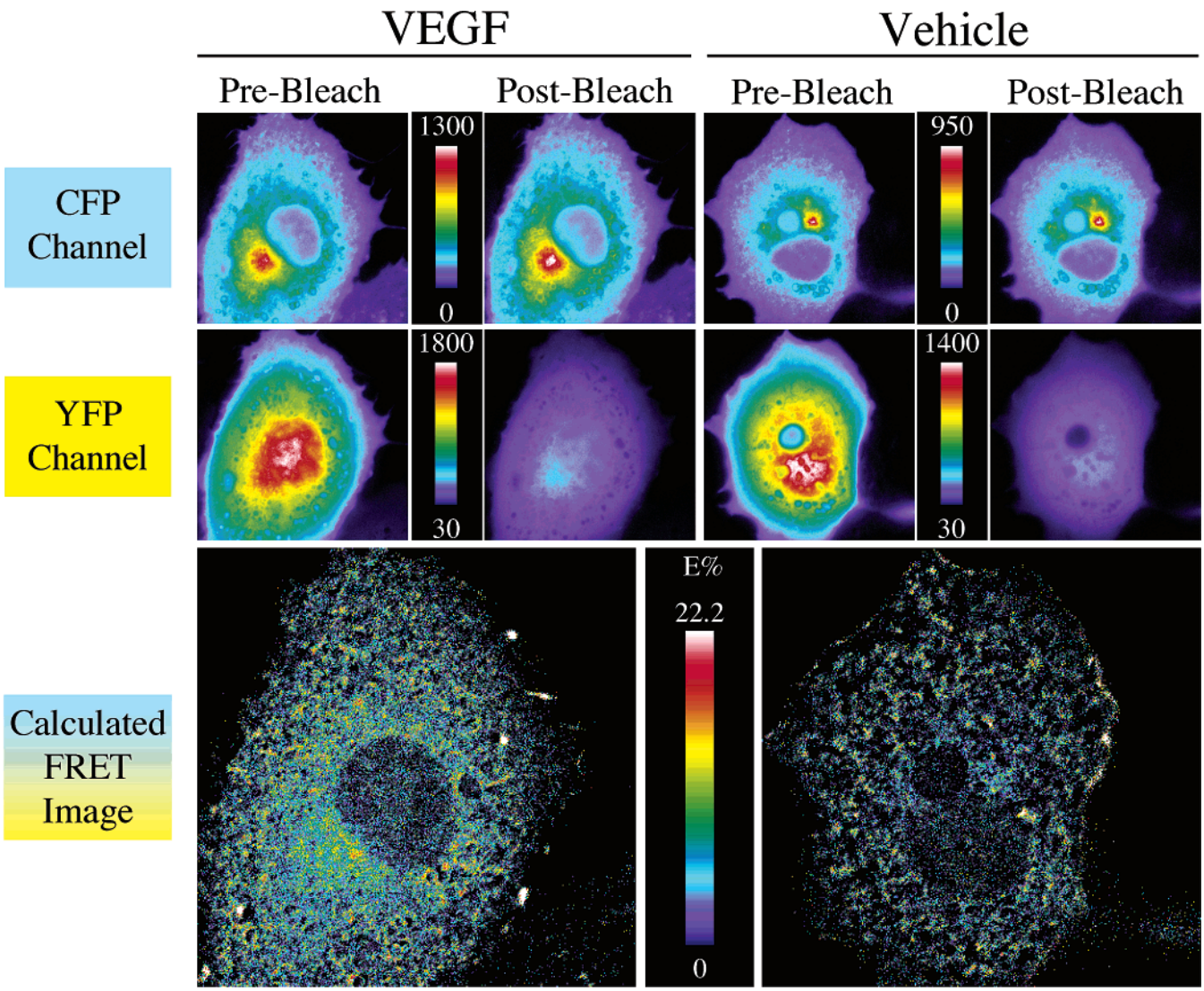

FIGURE 7: FRET imaging of eNOS−CaM interactions. BAEC were cotransfected with eNOS−ECFP and CaM−EYFP constructs and then analyzed for FRET following the addition of VEGF (20 ng/mL, left panels) or vehicle (right panels). These digital pseudocolor photomicrographs show that eNOS−ECFP fluorescence was present throughout the endothelial cell, with predominance in perinuclear membrane vesicles; this pattern was identical to that of the wild-type enzyme in these cells (*5*). CaM−EYFP fluorescence was present in both a cytoplasmic and a nuclear distribution. FRET images were obtained as described in the legend of Figure 4.

fected BAEC, in response to either VEGF or calcium ionophore.

Finally, we performed high-resolution FRET imaging experiments in BAEC cotransfected with eNOS−ECFP and calmodulin−EYFP. As shown in Figure 7, CaM−EYFP was expressed throughout the endothelial cell, most prominently in the cytosol. In contrast, eNOS−ECFP, like the wild-type enzyme (*5*), was localized in both internal and plasma membranes, with prominent expression in perinuclear vesicular structures (Figure 7). In response to VEGF, FRET between eNOS and calmodulin occurred at all sites of eNOS localization. These results indicated that all cellular eNOS populations were uniformly accessible to calmodulin after VEGF stimulation.

DISCUSSION

We have used FRET imaging methods to explore the spatiotemporal pattern of agonist-induced calcium mobilization and eNOS−calmodulin association in cultured live endothelial cells. These studies show that FRET imaging techniques can be applied successfully to the study of signaling protein interactions in living native cells. Although biochemical approaches to the analysis of signaling pathways have been highly informative, relatively few of the paradigms derived from studies using reconstituted or purified signaling proteins have been validated by analyses in living cells. The detection of intracellular FRET by the donor dequenching method may permit FRET imaging approaches to be extended broadly to the analysis of protein−protein interactions in native mammalian cells.

We have used an eNOS−cameleon chimera as an informative marker to analyze local calcium responses in the subcellular environments to which eNOS is localized (Figure 4). These studies show that, despite a heterogeneous pattern of subcellular eNOS distribution, calcium levels in the vicinity of eNOS rapidly increase throughout the cell in response to agonist activation. This result is consistent with our observation (Figure 7) that these same agonists promote the calcium-dependent interaction between eNOS and calmodulin throughout the same regions of the cell. These studies

also establish that eNOS throughout the cell is accessible to rapid changes in intracellular calcium concentration, and that subcellular calcium responses are identical to whole-cell calcium kinetics measured using Fluo-3 (Figure 2). Future experiments could use the eNOS−cameleon construct to analyze the spatial and temporal characteristics of local calcium responses in endothelial cells subjected to cellular perturbations, such as hemodynamic shear stress, in which the whole-cell calcium flux has a kinetic profile distinct from that induced by agonist stimulation.

Calmodulin, which mediates diverse calcium-regulated signaling pathways in a wide variety of cell types, represents one of the best-characterized intracellular signaling proteins (*11*). Although calmodulin-based reporter molecules and intramolecular FRET techniques have been used to measure intracellular calcium concentrations (*15*), much less is known about the interactions between calmodulin and its target proteins in intact cells. In endothelial cells, one major target for calmodulin is eNOS, which is itself a highly regulated signaling protein that plays an important role in blood pressure control and in the modulation of platelet aggregation. The interactions of eNOS with calmodulin have been characterized previously using biochemical approaches (*26*−*28*). These two key signaling proteins have different subcellular distributions and distinct modes of regulation, however. Here, we have used FRET methodologies to explore the spatial and temporal characteristics of agonist-regulated interactions between eNOS and calmodulin in living endothelial cells.

Because FRET between fluorophore-tagged proteins depends on both the proximity and the orientation of the donor and acceptor fluorophores, we designed a fusion protein in which the FRET fluorophore ECFP is introduced into eNOS immediately adjacent to the calmodulin-binding domain of the enzyme (Figure 1). Introducing a 28 kDa ECFP molecule into the middle of the 135 kDa eNOS protein does attenuate eNOS enzyme activity, but ∼10% of the wild-type eNOS activity is retained in this chimeric protein. We speculate that the region of the eNOS molecule near the calmodulin binding site serves as a molecular "hinge" between the C-terminal reductase domain and the N-terminal oxidase domain, and that this region has less stringent structural requirements than other regions of the protein that are directly implicated in catalysis and/or cofactor binding (*29*). The subcellular localization of both the eNOS−ECFP and ΔeNOS−ECFP fusion proteins is similar to that of wild-type eNOS, consistent with the fact that both of these chimeras contain the regions in the eNOS N-terminus that are required for targeting to plasmalemmal caveolae (*3*; see below). We designed the calmodulin−EYFP chimera to incorporate the fluorophore at the C-terminus of the calmodulin molecule. In this approach, we were guided by studies in which fusion proteins between calmodulin and flanking fluorophores retain their sensitivity to calcium (*15*), suggesting that these calmodulin chimeras are capable of folding properly. The calmodulin−EYFP chimera constructed here appears to be specific in its interaction with eNOS, because deletion of the calmodulin-binding domain from eNOS−ECFP leads to loss of the eNOS−calmodulin FRET signal (Figure 6).

In transfected endothelial cells, the CaM−EYFP construct is present throughout the endothelial cell (Figure 7), being most prominently expressed in the cytosol but also in the nucleus. In contrast, eNOS−ECFP, like the wild-type enzyme (*5*), is localized in both internal and plasma membranes, with prominent expression in perinuclear vesicular structures (Figure 7). Biochemical and hydrodynamic analyses have established that endothelial cell eNOS is targeted to plasma membrane caveolae (see reviews in refs *2* and *32*). These membrane microdomains are enriched with a variety of signaling proteins, including eNOS, calmodulin, and other proteins involved in cellular calcium homeostasis, receptors, heterotrimeric G proteins, and protein and lipid kinases (*33*, *34*). The localization of eNOS to caveolae may thus facilitate enzyme regulation by upstream activators that are also present in these structures, and influence the signaling pathways affected by NO once this mediator is synthesized by the enzyme. The scaffolding-regulatory protein caveolin is an important component of caveolae. This protein interacts directly with eNOS and inhibits enzyme activation, principally by attenuating the binding of calmodulin to eNOS (*3*, *28*). Immunofluorescence experiments have shown that caveolin, like eNOS, is found both in the plasma membrane and in perinuclear vesicular structures, suggesting that these internal membranes may represent internally disposed signaling domains (*5*). eNOS undergoes a dynamic translocation between the plasma membrane and internal membrane structures upon prolonged agonist stimulation (*5*), and some proportion of the eNOS present on intracellular membranes can be phosphorylated (*7*). Previous studies have failed to reveal, however, whether there are important differences in receptor responsiveness between eNOS at the plasma membrane and the enzyme at internal membranes. Our FRET image analyses show that eNOS localized in perinuclear membranes associates with calmodulin with a kinetic profile that is the same as that of eNOS at the plasma membrane.

Nagano and colleagues have used the NO-sensitive dye diaminofluorescein (DAF-2) to localize intracellular sites of NO synthesis (*30*, *31*), and have proposed that NO is synthesized throughout the cell (*7*). However, it is difficult to interpret observations using DAF-2 in terms of the intracellular localization of sites of NO synthesis, because this NO-sensitive dye forms a stable adduct with NO that appears to diffuse freely and rapidly throughout the cell, confounding conclusions about the localization of eNOS itself. Nonetheless, these results are consistent with these functional measurements of the level of intracellular NO generation.

In summary, these studies have used FRET methodologies to explore the interactions between eNOS and calmodulin in live BAEC. Our data provide evidence that the pool of rapidly responsive receptor-activated eNOS is distributed in both the plasma membrane and internal membranes of endothelial cells, and that this distribution parallels the localization of agonist-induced changes in intracellular Ca^{2+} levels in the vicinity of eNOS. The spatial heterogeneity of the distribution of eNOS within the endothelial cell may reflect the existence of distinct subcellular or extracellular targets for NO, which may undergo coordinated activation in response to extracellular signals in the vascular wall.

ACKNOWLEDGMENT

We thank Jennifer W. Shuler, Marc Damelin, and Pamela Silver for access to their sophisticated microscope systems

and for expert advice on the use of these systems. Figure 3 was obtained in the Nikon Imaging Center at Harvard Medical School.

REFERENCES

1. Fleming, I., and Busse, R. (2003) Molecular mechanisms involved in the regulation of the endothelial nitric oxide synthase, *Am. J. Physiol. 284*, R1−R12.
2. Michel, T., and Feron, O. (1997) Nitric oxide synthase: which, where, how, and why? *J. Clin. Invest. 100*, 2146−2152.
3. Ju, H., Zou, R., Venema, V. J., and Venema, R. C. (1997) Direct interaction of endothelial nitric-oxide synthase and caveolin-1 inhibits synthase activity, *J. Biol. Chem. 272*, 18522−18525.
4. Shaul, P. W. (2002) Regulation of endothelial nitric oxide synthase: location, location, location, *Annu. Rev. Physiol. 64*, 749−774.
5. Prabhakar, P., Thatte, H. S., Goetz, R. M., Cho, M. R., Golan, D. E., and Michel, T. (1998) Receptor-regulated translocation of endothelial nitric-oxide synthase, *J. Biol. Chem. 273*, 27383−27388.
6. Gonzalez, E., Kou, R., Lin, A. J., Golan, D. E., and Michel, T. (2002) Subcellular targeting and agonist-induced site-specific phosphorylation of endothelial nitric-oxide synthase, *J. Biol. Chem. 277*, 39554−39560.
7. Fulton, D., Fontana, J., Sowa, G., Gratton, J. P., Lin, M., Li, K. X., Michell, B., Kemp, B. E., Rodman, D., and Sessa, W. C. (2002) Localization of endothelial nitric-oxide synthase phosphorylated on serine 1179 and nitric oxide in Golgi and plasma membrane defines the existence of two pools of active enzyme, *J. Biol. Chem. 277*, 4277−4284.
8. Govers, R., and Rabelink, T. J. (2001) Cellular regulation of endothelial nitric oxide synthase, *Am. J. Physiol. 280*, F193−F206.
9. Alderton, W. K., Cooper, C. E., and Knowles, R. G. (2001) Nitric oxide synthases: structure, function and inhibition, *Biochem. J. 357*, 593−615.
10. Fleming, I., and Busse, R. (1999) Signal transduction of eNOS activation, *Cardiovasc. Res. 43*, 532−541.
11. Klee, C. B., Crouch, T. H., and Richman, P. G. (1980) Calmodulin, *Annu. Rev. Biochem. 49*, 489−515.
12. Chan, F. K., Siegel, R. M., Zacharias, D., Swofford, R., Holmes, K. L., Tsien, R. Y., and Lenardo, M. J. (2001) Fluorescence resonance energy transfer analysis of cell surface receptor interactions and signaling using spectral variants of the green fluorescent protein, *Cytometry 44*, 361−368.
13. Kenworthy, A. K. (2001) Imaging protein−protein interactions using fluorescence resonance energy transfer microscopy, *Methods 24*, 289−296.
14. Gordon, G. W., Berry, G., Liang, X. H., Levine, B., and Herman, B. (1998) Quantitative fluorescence resonance energy transfer measurements using fluorescence microscopy, *Biophys. J. 74*, 2702−2713.
15. Miyawaki, A., Llopis, J., Heim, R., McCaffery, J. M., Adams, J. A., Ikura, M., and Tsien, R. Y. (1997) Fluorescent indicators for Ca^{2+} based on green fluorescent proteins and calmodulin, *Nature 388*, 882−887.
16. Tsien, R. Y. (1998) The green fluorescent protein, *Annu. Rev. Biochem. 67*, 509−544.
17. Robinson, L. J., and Michel, T. (1995) Agonist-modulated palmitoylation of endothelial nitric oxide synthase, *Proc. Natl. Acad. Sci. U.S.A. 92*, 11776−11780.
18. Igarashi, J., and Michel, T. (2000) Agonist-modulated targeting of the EDG-1 receptor to plasmalemmal caveolae: eNOS activation by sphingosine 1-phosphate and the role of caveolin-1 in sphingolipid signal transduction, *J. Biol. Chem. 275*, 32363−32370.
19. Lamas, S., Marsden, P. A., Li, G. K., Tempst, P., and Michel, T. (1992) Endothelial nitric oxide synthase: molecular cloning and characterization of a distinct constitutive enzyme isoform, *Proc. Natl. Acad. Sci. U.S.A. 89*, 6348−6352.
20. Feron, O., Michel, J. B., Sase, K., and Michel, T. (1998) Dynamic regulation of endothelial nitric oxide synthase: complementary roles of dual acylation and caveolin interactions, *Biochemistry 37*, 193−200.
21. Damelin, M., and Silver, P. A. (2000) Mapping interactions between nuclear transport factors in living cells reveals pathways through the nuclear pore complex, *Mol. Cell 5*, 133−140.
22. Kenworthy, A. K., and Edidin, M. (1998) Distribution of a glycosylphosphatidylinositol-anchored protein at the apical surface of MDCK cells examined at a resolution of <100 Å using imaging fluorescence resonance energy transfer, *J. Cell Biol. 142*, 69−84.
23. He, H., Venema, V. J., Gu, X., Venema, R. C., Marrero, M. B., and Caldwell, R. B. (1999) Vascular endothelial growth factor signals endothelial cell production of nictric oxide and prostacyclin through flk-1/KDR activation of c-Src, *J. Biol. Chem. 274*, 25130−25135.
24. Kantor, D. B., Lanzrein, M., Stary, S. J., Sandoval, G. M., Smith, W. B., Sullivan, B. M., Davidson, N., and Schuman, E. M. (1996) A role for endothelial NO synthase in LTP revealed by adenovirus-mediated inhibition and rescue, *Science 274*, 1744−1748.
25. Igarashi, J., and Michel, T. (2001) Sphingosine 1-phosphate and isoform-specific activation of phosphoinositide 3-kinase beta. Evidence for divergence and convergence of receptor-regulated endothelial nitric-oxide synthase signaling pathways, *J. Biol. Chem. 276*, 36281−36288.
26. Venema, R. C., Sayegh, H. S., Arnal, J. F., and Harrison, D. G. (1995) Role of the enzyme calmodulin-binding domain in membrane association and phospholipid inhibition of endothelial nitric oxide synthase, *J. Biol. Chem. 270*, 14705−14711.
27. Michel, J. B., Feron, O., Sacks, D., and Michel, T. (1997) Reciprocal regulation of endothelial nitric oxide synthase by Ca^{2+}-calmodulin and caveolin, *J. Biol. Chem. 272*, 15583−15586.
28. Michel, J. B., Feron, O., Sase, K., Prabhakar, P., and Michel, T. (1997) Caveolin versus calmodulin, *J. Biol. Chem. 272*, 25907−25912.
29. Raman, C. S., Li, H., Martasek, P., Kral, V., Masters, B. S., and Poulos, T. L. (1998) Crystal structure of constitutive endothelial nitric oxide synthase: a paradigm for pterin function involving a novel metal center, *Cell 95*, 939−950.
30. Kojima, H., Sakurai, K., Kikuchi, K., Kawahara, S., Kirino, Y., Nagoshi, H., Hirata, Y., and Nagano, T. (1998) Development of a fluorescent indicator for nitric oxide based on the fluorescein chromophore, *Chem. Pharm. Bull. 46*, 373−375.
31. Nakatsubo, N., Kojima, H., Kikuchi, K., Nagoshi, H., Hirata, Y., Maeda, D., Imai, Y., Irimura, T., and Nagano, T. (1998) Direct evidence of nitric oxide production from bovine aortic endothelial cells using new fluorescence indicators−diaminofluoresceins, *FEBS Lett. 427*, 263−266.
32. Shaul, P. W., and Anderson, R. G. W. (1998) Role of plasmalemmal caveolae in signal transduction, *Am. J. Physiol. 275*, L843−L851.
33. Lisanti, M. P., Scherer, P. E., Vidugiriene, J., Tang, Z., Hermanowski-Vosatka, A., Tu, Y. H., Cook, R. F., and Sargiacomo, M. (1994) Characterization of caveolin-rich membrane domains isolated from an endothelial-rich source: implications for human disease, *J. Cell Biol. 126*, 111−126.
34. Okamoto, T., Schlegel, A., Scherer, P. E., and Lisanti, M. P. (1998) Caveolins, a family of scaffolding proteins for organizaing "preassembled signaling complexes" at the plasma membrane, *J. Biol. Chem. 273*, 5419−5422.

BI035066W